Supporting Information

The Stratified Microbial Carbon Pump: Thermal Stratification Enhances Refractory Dissolved Organic Carbon Production and Stabilizes Carbon in Alkaline Karst Waters through Keystone Microbial Interaction Networks

Yikun Jia[1,2], Junbing Pu[3*], Zaihua Liu[1**], Qiufang He[4], Xinlu Su[3], Tao Zhang[3], Jianhong Li[5], Sibo Zeng[1]

1. State Key Laboratory of Environmental Geochemistry, Institute of Geochemistry, Chinese Academy of Sciences (CAS), Guiyang 550081, China

2. University of Chinese Academy of Sciences, Beijing 100049, China

3. Karst Research Team, Chongqing Key Laboratory of Carbon cycle and Carbon regulation of Mountain Ecosystem, School of Geography and Tourism, Chongqing Normal University, Chongqing, 401331, China

4. Chongqing Key Laboratory of Karst Environment & School of Geographical Sciences, Southwest University, Chongqing 400700, China

5. Key Laboratory of Karst Dynamics, MNR & Guangxi, Institute of Karst Geology, Chinese Academy of Geological Sciences, Guilin, China

** Corresponding author：Junbing Pu*

Address：School of Geography and Tourism, Chongqing Normal University, NO.37, Daxuecheng Central Road, University Town Campus, Shapingba District, Chongqing, 401331, P. R. China

E-mail: junbingpu@163.com

*** Corresponding author Zaihua Liu*
Address: State Key Laboratory of Environmental Geochemistry, Institute of Geochemistry, Chinese Academy of Sciences (CAS), NO.99, West Lincheng Road, Guanshanhu District, Guiyang, 550081, China.
E-mail: liuzaihua@vip.gyig.ac.cn.

Text S1. Spatial Variation Characteristics of Hydrochemical Parameters

The WT, pH, and DO reach their highest levels during the OTS period, with mean values of 27.81 ± 3.27 °C, 7.84 ± 0.85, and 5.45 ± 3.16 mg/L, respectively. In contrast, the Chl-a concentration peaked during the ITS period, averaging 5.48 ± 2.75 μg/L, while all hydrochemical parameters were relatively low during the MX period **(Fig. S1)**. Analysis of water quality indicators in DLD Reservoir showed that the highest mean TN concentration occurred during OTS period (1.21 ± 0.80 mg/L), followed by MX period (1.00 ± 0.34 mg/L) and ITS period (0.71 ± 0.27 mg/L). For TP, the mean concentrations were highest during OTS and MX periods (0.09 ± 0.02 mg/L and 0.09 ± 0.01 mg/L, respectively), and lowest during ITS periods (0.06 ± 0.02 mg/L) **(Fig. S1)**. Although the mean Chl-a concentration (5.48 ± 2.75 μg/L) and DO levels (5.45 ± 3.16 mg/L) may appear relatively moderate compared to eutrophic systems, they do not negate the dominance of autochthonous DOM as indicated by HIX and β:α ratios. In karst reservoirs, the high availability of DIC can decouple primary production from biomass accumulation. The relatively low standing crop of Chl-a, coupled with moderate DO, suggests a high turnover rate of autochthonous carbon rather than low productivity. In this scenario, the abundant DIC fuels rapid photosynthetic carbon fixation, which is then swiftly processed by the active microbial community—evidenced by the cohesive bacterial networks observed—into the RDOC. Furthermore, the lower DO levels, particularly during periods of high nutrient availability (TN and TP peaking in OTS), likely reflect intense heterotrophic respiration. This microbial activity consumes dissolved oxygen while simultaneously facilitating the transformation of labile autochthonous carbon into refractory humic-like components (the MCP process). Thus, the optical signatures (low HIX and high β:α) reflect the fresh, microbial-mediated nature of the DOM pool, while the modest Chl-a and DO values represent a dynamic equilibrium where carbon is efficiently shunted from the labile pool into long-term RDOC storage.

Significant vertical variations in hydrochemical parameters were observed during both the incubating and obvious thermal stratification periods **(Fig. S1)**. During thermal stratification, these parameters generally decreased gradually along the vertical profile from the thermocline to the hypolimnion, where the minimum values were recorded. In contrast, during the MX period, hydrochemical indicators showed almost no vertical variation, with the exception of a slight localized increase in Chl-a in the lower hypolimnion of the upstream section. Vertically, TN concentrations during both stratified periods exhibited the pattern: hypolimnion > thermocline > epilimnion. During the MX period, the vertical gradient in TN was less pronounced, though concentrations remained highest in the hypolimnion, followed by the epilimnion and thermocline. Similarly, TP concentrations showed minimal variation across layers during the mixing period due to the absence of thermal stratification. Under stratified conditions, however, TP followed the same spatial trend as TN: hypolimnion > thermocline > epilimnion. Overall, across all study periods, the hypolimnion exhibited the most pronounced eutrophication status in DLD Reservoir.

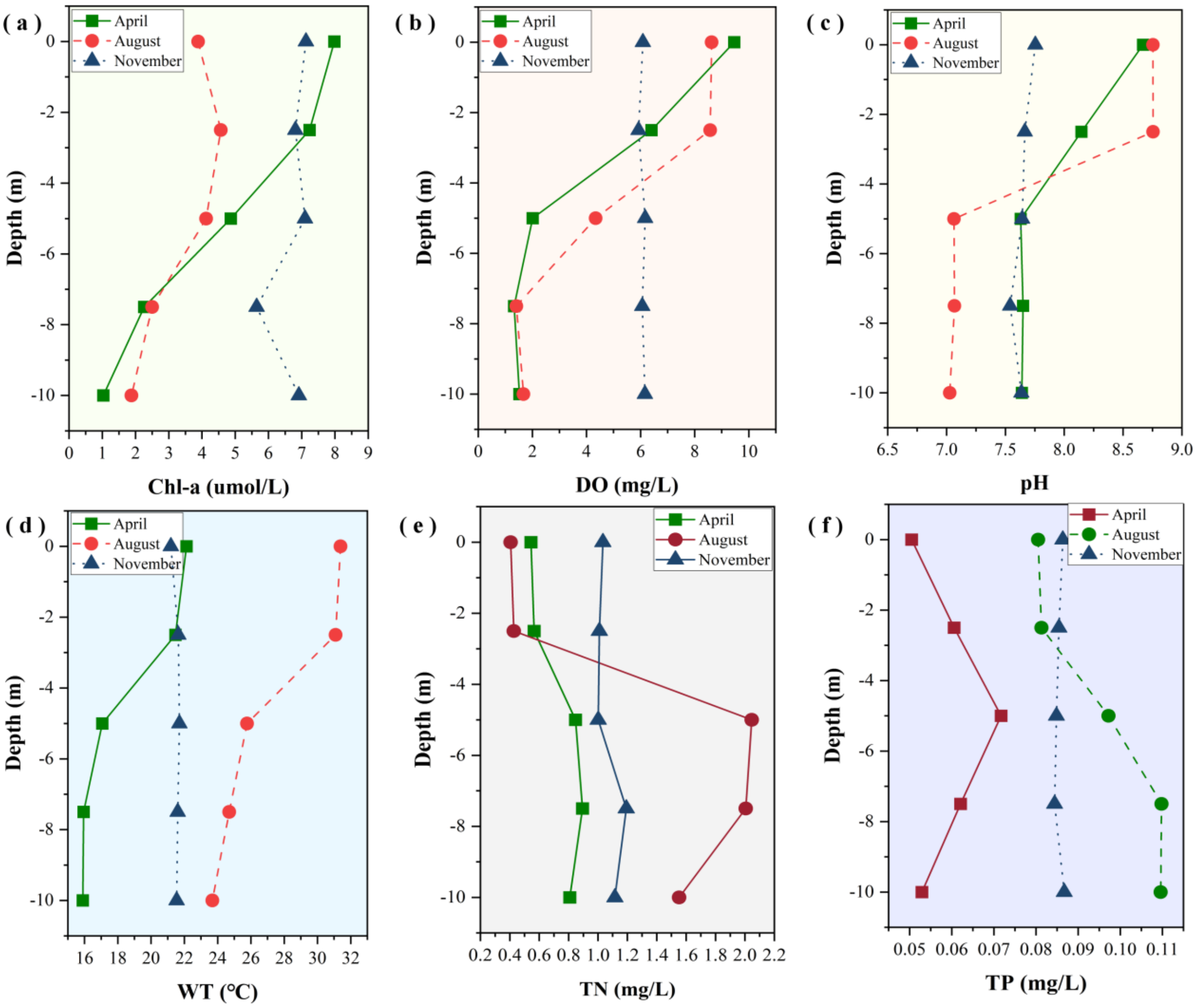

Fig.S1 Spatial and temporal variations of water chemistry indicators in DLD Reservoir during different periods of time

Text S2. Analysis of DOM Features

Through proportional analysis of DOC components across different water layers during the ITS, OTS, and MX periods, the following distribution characteristics were observed: During the ITS period, LDOC and SLDOC accounted for 84% and 16% respectively in the epilimnion; 71% and 29% in the thermocline; and 79% and 21% in the hypolimnion. In the OTS period, RDOC was detected in all layers: the epilimnion showed LDOC 83%, SLDOC 0%, and RDOC 17%; the thermocline contained 60% LDOC, 16% SLDOC, and 24% RDOC; while the hypolimnion had 58% LDOC, 16% SLDOC, and 26% RDOC. By the MX period, the DOC composition shifted significantly: no LDOC was detected in the epilimnion where SLDOC and RDOC accounted for 55% and 45% respectively; similarly, the thermocline showed no LDOC with SLDOC and RDOC at 52% and 48%; while the hypolimnion contained 28% LDOC, 27% SLDOC, and 45% RDOC.

According to the concentration formula **Equation. S1**, distinct concentration patterns emerged across periods and layers: In the ITS period, LDOC and SLDOC concentrations of the epilimnion were 2.59 mg/L and 0.49 mg/L; thermocline levels were 1.90 mg/L and 0.78 mg/L; while hypolimnion concentrations reached 3.33 mg/L and 0.62 mg/L. During OTS period, RDOC began appearing with epilimnion LDOC and SLDOC at 6.48 mg/L and 1.33 mg/L (RDOC undetected); thermocline concentrations were LDOC 3.12 mg/L, SLDOC 1.25 mg/L, and RDOC 0.83 mg/L; hypolimnion levels were LDOC 2.47 mg/L, SLDOC 1.11 mg/L, and RDOC 0.68 mg/L. The MX period showed marked changes: no LDOC detected in epilimnion where RDOC and SLDOC measured 1.57 mg/L and 1.28 mg/L; thermocline similarly showed no LDOC with RDOC and SLDOC at 1.42 mg/L and 1.31 mg/L; while hypolimnion concentrations were LDOC 0.74 mg/L, SLDOC 0.71 mg/L, and RDOC 1.19 mg/L.

RDOC (mg/L) = DOC × RDOC (%)

LDOC (mg/L) = DOC × LDOC (%)

SLDOC (mg/L) = DOC × SLDOC (%) **（Equation. S1）**

Table S1. Excitation and emission of PARAFAC components.

Component	Ex/Em (nm)	Type	References
C1	250 ~ 300/430 ~ 450	SLDOC	300 ~ 350/400 ~ 600 **(Garcia et al., 2015)**
C2	230 ~ 240/330 ~ 350	LDOC	210 ~ 240/330 ~380; 200 ~ 215/330 ~ 345 **(He et al., 2021; Lee et al., 2018)**
C3	270 ~ 280 (<240)/330 ~ 370	LDOC	270 ~ 295/330 ~ 380; 240, 310/340 **(He et al., 2021)**
C4	235 ~ 240/398 ~ 420	RDOC	240(310)/420 **(Weiying et al., 2013)**
C5	200/290	LDOC	220 (255)/290; 200/285 **(Zhou et al., 2013; Bianchi et al., 2014)**

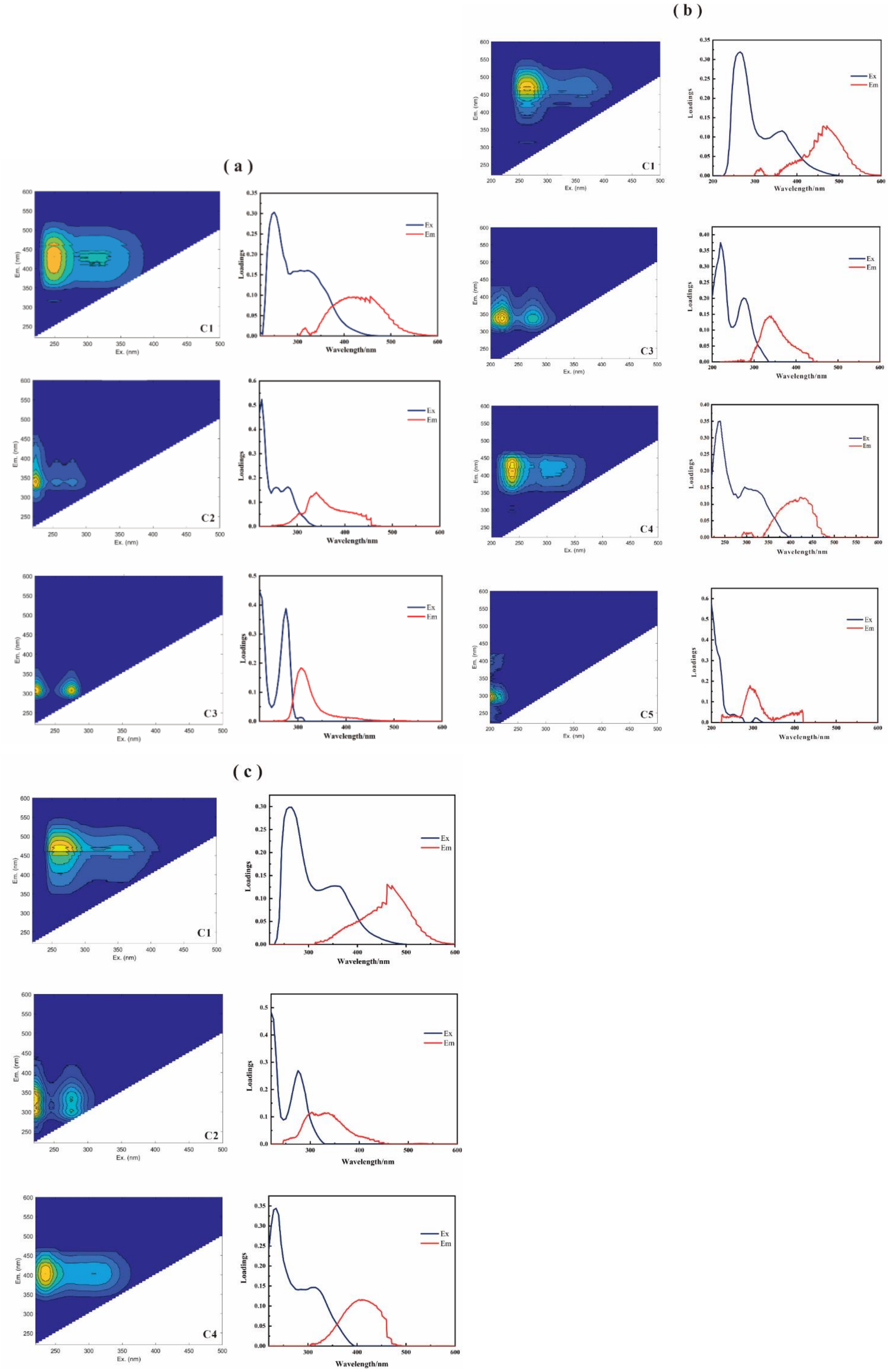

Fig. S2 DOM components and the loading map for the ITS period (April) (a), the OTS period (August) (b), and the MX period (November) (c).

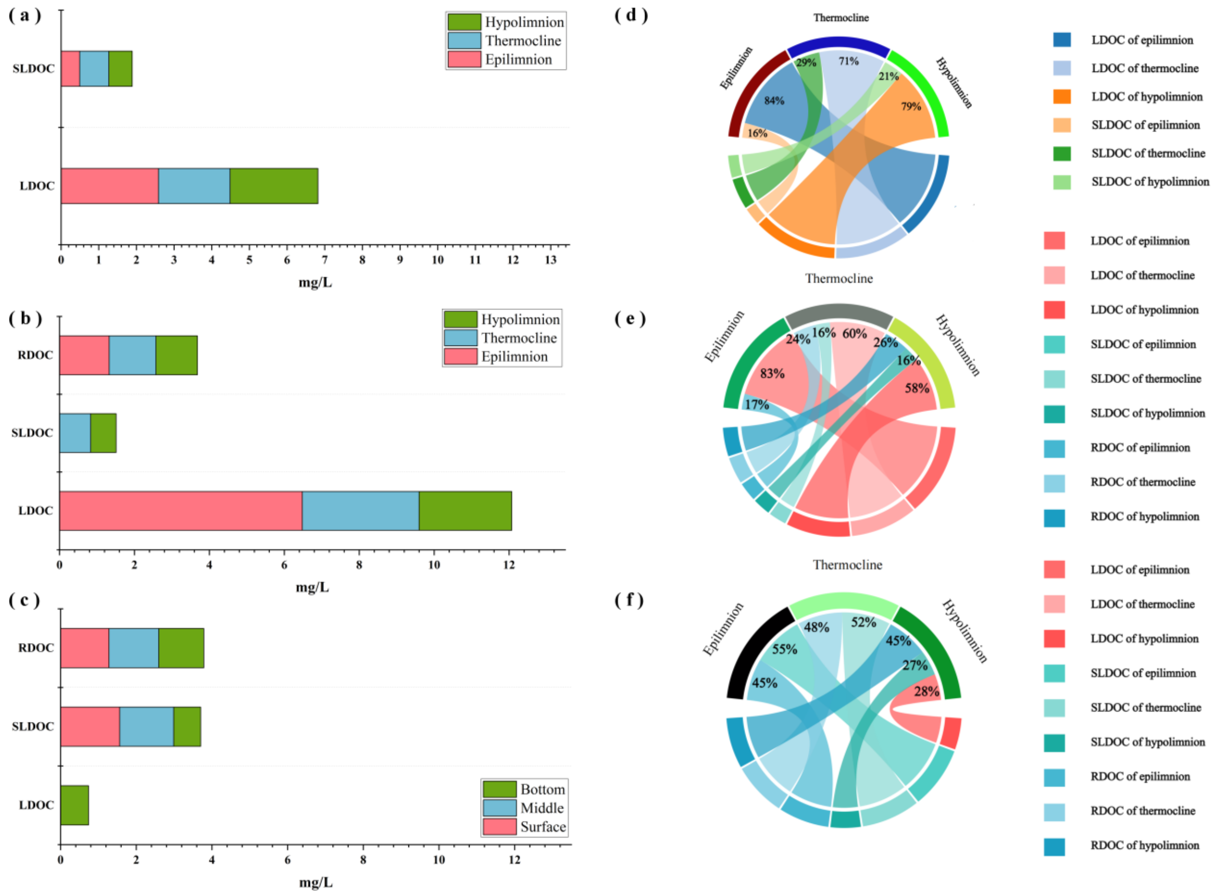

Fig. S3 Spatial variations in the concentrations and proportions of DOC components in the DLD reservoir during the ITS period (a and d), the OTS period (b and e), and the MX period (c and f).

Text S3. Spatial and Temporal Variation Characteristics of Spectral Parameters

The optical properties of DOM exhibited distinct stage-specific variations across the three hydrological periods (ITS, OTS, and MX periods). The average HIX values were 1.00 ± 0.51, 2.00 ± 0.71, and 3.55 ± 0.88, respectively, indicating a progressive increase in the degree of DOM humification from the incubation to the MX period **(Zsolnay et al., 1999; Ohno, 2002)**. The highest value during MX period suggests the presence of more complex and stable organic matter, likely resulting from increased terrestrial inputs or accumulation of microbial degradation products. The FI averaged 2.35 ± 0.60, 2.21 ± 0.14, and 2.14 ± 0.06, showing a slight decreasing trend while remaining above 1.9, which reflects a predominantly autochthonous biological origin of DOM **(McKnight et al., 2001)**. Over time, microbial activity or photodegradation may have slightly attenuated its autochthonous character. Given the predominantly autochthonous nature of the DOM **(Parlanti et al., 2000)**, we propose that much of the humic-like material during the MX period likely originated from accumulated biological transformation processes occurring in the OTS period. The β:α ratio averaged 0.99 ± 0.51, 1.02 ± 0.21, and 1.00 ± 0.03 across the three periods, with minimal variation, indicating relative temporal stability in the autochthonous signature of DOM, though spatial differences in intensity may exist **(Parlanti et al., 2000; Huguet et al., 2009)**. In contrast, the spectral slope ratio (SR) decreased markedly from 0.96 ± 0.63 (ITS period) and 0.81 ± 0.32 (OTS period) to 0.35 ± 0.17 (MX period), indicating a significant increase in DOM molecular weight and enhanced aromaticity during the MX period **(Helms et al., 2008)**, likely associated with intensified water column mixing, resuspension of particulate organic matter, or allochthonous inputs. Collectively, these parameter shifts reveal a dynamic evolution in DOM source and composition across different hydrological phases, with the MX period characterized by elevated humification and higher molecular weight, signaling a notable environmentally driven transition.

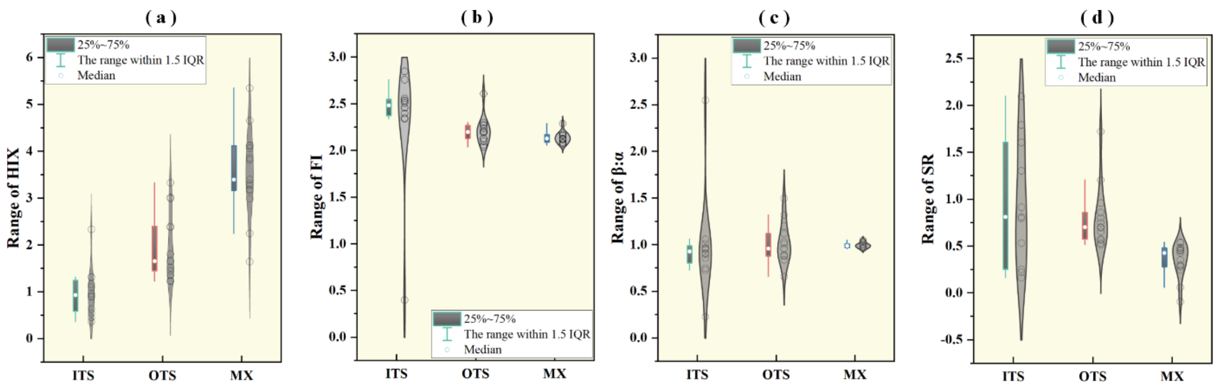

Fig. S4 Temporal variations in spectral parameters HIX (a), FI (b), β:α (c), and SR (d) across the ITS, OTS, and MX periods.

Vertical variations of spectral parameters across different periods are shown in **Fig. S5**. During the ITS period, HIX gradually increased within the 0 – 5 m depth range, peaking at 5 m (1.34), and then decreased markedly between 7.5 m and 10 m, indicating a higher degree of organic matter humification in the thermocline relative to the surface and bottom layers. FI exhibited minimal overall variation, with a maximum value (2.71) at 5 m, suggesting a relatively high contribution of autochthonous organic matter at this depth. Apart from an anomalous value at 7.5 m, FI remained relatively consistent across depths. SR gradually decreased from the surface to 5 m, increased markedly to 1.45 at 7.5 m, and then decreased again by 10 m. The β:α ratio continuously decreased from the surface to a minimum of 0.69 at 5 m, followed by a slight recovery.

In the OTS period, HIX increased consistently from the surface to 7.5 m, reaching a maximum of 2.57 at 7.5 m, indicating a significant enhancement in organic matter humification with depth and notable accumulation of humic-like substances in the middle and bottom layers.

FI ranged between 2.09 and 2.41, showing a slight increasing trend with depth and reaching its highest value (2.41) in the bottom layer. SR decreased gradually from the surface, reaching a minimum of 0.60 at 5 m before recovering slightly, reflecting relatively higher molecular weight or aromaticity of DOM in the middle layer, potentially associated with intensified degradation. The β:α ratio peaked at 1.16 at 2.5 m and then gradually declined, suggesting higher biological activity or freshness of organic matter around this depth, with increased aging or degradation toward the bottom.

During the MX period, HIX showed elevated values at both 2.5 m and 10 m, reaching a maximum of 3.97 in the bottom layer, indicating significant accumulation and advanced humification of organic matter in the sediments. FI varied only slightly throughout the water column (2.09 - 2.17), indicating a consistent DOM source and uniform distribution of microbial or autochthonous contributions across depths without clear stratification. SR values were generally low (0.25 - 0.44) with no consistent vertical trend, reaching a minimum at 5 m, which reflects higher molecular weight and aromaticity of DOM at this depth. The β:α ratio remained highly stable across all depths, consistently close to 1, indicating minimal variation in the biological activity or freshness of organic matter from surface to bottom.

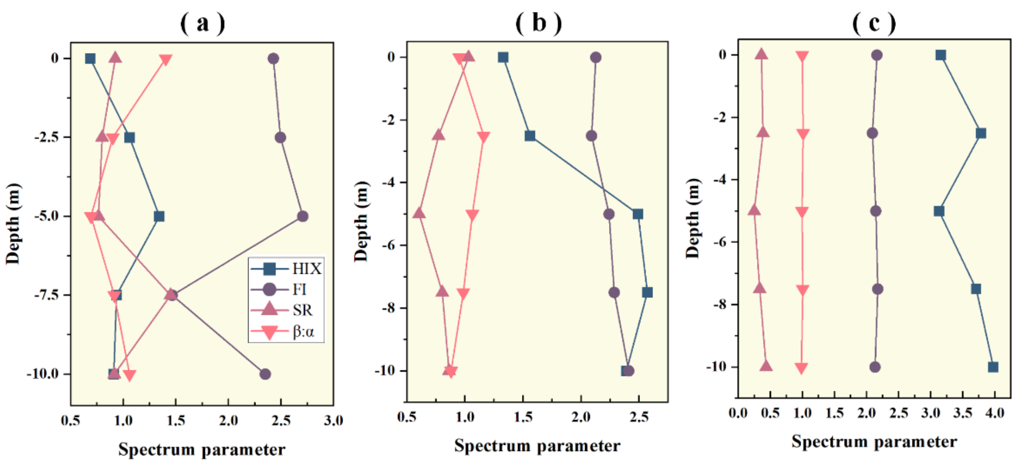

Fig. S5 Spatial variations of spectral parameters HIX, FI, β:α, and SR during the ITS (a),

OTS (b), and MX (c) periods.

Text S4. Formulas and Parameters for Thermal Stratification Calculation in the DLD Reservoir

The identification of TS and MX periods requires the calculation of stratification indices. These include the *Schmidt Stability Index (SSI)*, the water column stability index *RWCS/H* **(Shi et al., 2016)**, and the depths of the upper and lower boundaries of the thermocline. The SSI and thermocline boundary depths were computed using the R package *rLakeAnalyzer* (https://rdrr.io/cran/rLakeAnalyzer/). According to Idso **(1973)** , the *SSI* quantifies the work required per unit area to homogenize the density profile of a lake or reservoir without adding or removing heat. During thermal stratification, significant density differences exist between water layers at different depths, resulting in higher *SSI* values. The input data required for these calculations include the reservoir surface area, water depth, water temperature profiles, and other factors, with *SSI* expressed in units of J/m^2 . The *SSI* is calculated using **Equation. S2**:

$$SSI = A_0^{-1} \sum_{Z_0}^{Z_m} (Z - Z_\rho)(\rho_Z - \bar{\rho}) A_Z \Delta z \quad \textbf{(Equation. S2)}$$

where Z denotes depth, Z_ρ represents the mean density at depth Z, Z_m is the maximum depth of the reservoir, and ΔZ is the depth interval of measurement.

The *RWCS/H* index provides an effective measure of the stability of thermal stratification in the water column and is calculated using **Equation. S3**:

$$RWCS/H = \frac{D_b - D_s}{(D_4 - D_5) * H} \quad \textbf{(Equation. S3)}$$

where D_b and D_s represent the density of the bottom and surface water layers, respectively, in $kg \cdot m^{-3}$; D_4 and D_5 denote the density of pure water at 4 °C and 5 °C, respectively, in $kg \cdot m^{-3}$;

and *H* is the water depth in m.

The water density calculation formula follows Lawson and Anderson **(2007)**:

$$\rho_t = 1000 \times [1 - \frac{T+288.9414}{508929.2(T+68.12936)} \times (T - 3.9863)^2] \quad \textbf{(Equation. S4)}$$

ρ_t denotes the density of surface water; T represents the water temperature in degrees ℃.

The calculated SSI values for April, August, and November, derived using **Equations. S2 and S3**, were 94.03, 165.61, and -2.99, respectively. The corresponding mean *RWCS/H* values were 19.58, 32.19, and -0.94. Both the *SSI* and *RWCS/H* indices showed consistent trends, with values in August exceeding those in April, which were in turn higher than those in November. The negative values observed in November align with the vertical water temperature profile characteristics.

Text. S5 The primary categories and abundance of Keystone taxa

Phylogenetic annotation revealed that *Proteobacteria*, *Bacteroidetes*, *Planctomycetes*, and *Firmicutes* constituted the keystone taxa during the ITS period in the reservoir, accounting for 60.9% of all putative keystone taxa. During the OTS period, *Actinobacteria*, *Proteobacteria*, and *Cyanobacteria* were identified as the keystone taxa, representing 78.6% of the total. In the MX period, the keystone taxa were dominated by *Proteobacteria*, *Bacteroidetes*, and *Verrucomicrobia*, collectively comprising 81.8% of all putative keystone taxa. *Proteobacteria* consistently functioned as Module hubs across the ITS, OTS, and MX periods, though the specific genera contributing to this role varied among the study periods. During the ITS period, keystone taxa within *Proteobacteria* primarily included *Sulfurimonas*, *Sterolibacterium*, *Denitratisoma*, *Candidatus Nitrotoga*, *Rubrivivax*, and the *MWH-UniP1 aquatic group*. In the OTS period, *Proteobacteria* were relatively less represented among keystone taxa, with *Limnobacter* and *Sphaerotilus* being the main genera. Notably, four OTUs affiliated with the actinobacterial genus *CL500-29 marine group* were identified as keystone taxa during this period. In the MX period, keystone taxa within *Proteobacteria* included *Paucibacter*, *Candidatus Methylopumilus*, and *Limnibacter*. The only two Network hubs observed, both occurring during the OTS period, belonged to the genus *hgcI clade* (*Actinobacteria*) and the genus *Terrimonas* (*Bacteroidetes*).

Text. S6 Spatio-temporal variations in bacterial positive and negative cohesive values

In DLD Reservoir **(Table. S2),** positive cohesion varied considerably across layers during ITS and MX periods but remained stable during OTS. The highest mean positive cohesion (0.50) occurred in the thermocline during ITS. Spatially, positive cohesion during ITS first increased then decreased with depth, showed a slight increasing trend during OTS, and was lowest in the middle layer during MX. Negative cohesion differed little across layers during ITS and OTS but was relatively high in the surface layer (-0.40) during MX. Temporally, mean positive cohesion was significantly higher during ITS (0.41 ± 0.02) and OTS (0.43 ± 0.03) than during MX (0.29 ± 0.01). Similarly, mean negative cohesion was stronger during stratified periods than during MX.

Table. S2 Spatiotemporal variations in positive and negative bacterial cohesion parameters in the water column.

Period	Layers	Positive Cohesion	Negtive Cohesion
ITS period	Epilimnion	0.41	-0.40
	Thermocline	0.50	-0.40
	Hypolimnion	0.40	-0.37
OTS period	Epilimnion	0.43	-0.41
	Thermocline	0.44	-0.40
	Hypolimnion	0.47	-0.44
MX period	Surface layer	0.42	-0.40
	Middle layer	0.32	-0.31
	Bottom layer	0.41	-0.37

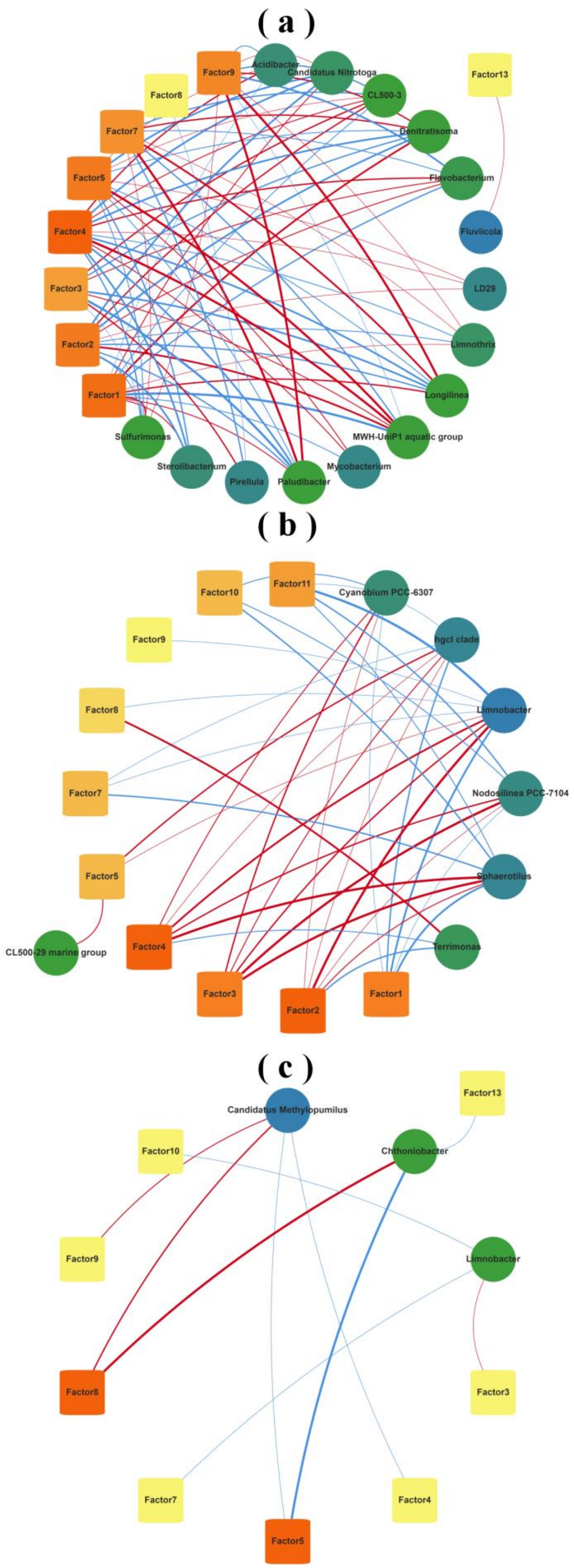
(a)
Factor9
Acidibacter
Candidatus Nitrotoga
CL500-3
Factor13
Factor8
Factor7
Denitratisoma
Factor5
Flavobacterium
Factor4
Fluviicola
Factor3
LD29
Factor2
Limnothrix
Factor1
Longilinea
Sulfurimonas
MWH-UniP1 aquatic group
Sterolibacterium
Pirellula
Paludibacter
Mycobacterium
(b)
Factor10
Factor11
Cyanobium PCC-6307
Factor9
hgcI clade
Factor8
Limnobacter
Factor7
Nodosilinea PCC-7104
Factor5
Sphaerotilus
CL500-29 marine group
Factor4
Terrimonas
Factor3
Factor2
Factor1
(c)
Candidatus Methylopumilus
Factor13
Factor10
Chthoniobacter
Factor9
Limnobacter
Factor8
Factor3
Factor7
Factor4
Factor5

Fig. S6 Relationships between the relative abundance of keystone taxa and environmental factors during the (a) ITS period, (b) OTS period, and (c) MX period. Factor designations: Factor1, bicarbonate concentration; Factor2, water temperature; Factor3, pH; Factor4, DO; Factor5, Chl-a; Factor6, δ13C$_{DIC}$; Factor7, pCO$_2$; Factor8, TP; Factor9, TN; Factor10, HIX; Factor11, FI; Factor12, SR; Factor13, β:α ratio. Red lines indicate positive correlations, blue lines indicate negative correlations, and thicker lines represent higher correlation coefficients.

Table S3. The co-occurrence network parameters of bacteria during the ITS period, OTS period and MX period.

	ITS	**OTS**	**MX**
Nodes num	352	549	432
Edges num	6403	34564	6558
Positive.cor num	4160	21212	4780
Negative.cor num	2243	13352	1778
Network density	0.103	0.230	0.070
Clustering coefficient	0.567	0.670	0.555

References

Bianchi T. S., Osburn C., Shields M. R., Yvon-Lewis S., Young J., Guo L., Zhou Z., 2014. Deepwater Horizon Oil in Gulf of Mexico Waters after 2 Years: Transformation into the Dissolved Organic Matter Pool. Environmental Science & Technology. 48 (16): 9288-9297.

Garcia R. D., Reissig M., Queimaliños C. P., Garcia P. E., Dieguez M. C., 2015. Climate-driven terrestrial inputs in ultraoligotrophic mountain streams of Andean Patagonia revealed through chromophoric and fluorescent dissolved organic matter. Science of The Total Environment. 521-522: 280-292.

He Q., Xiao Q., Fan J., Zhao H., Cao M., Zhang C., Jiang Y., 2021. Excitation-emission matrix fluorescence spectra of chromophoric dissolved organic matter reflected the composition and origination of dissolved organic carbon in Lijiang River, Southwest China. Journal of Hydrology. 598: 126240.

Helms J. R., Stubbins A., Ritchie J. D., Minor E. C., Kieber D. J., Mopper K., 2008. Absorption spectral slopes and slope ratios as indicators of molecular weight, source, and photobleaching of chromophoric dissolved organic matter. Limnology and Oceanography. 53 (3): 955-969.

Huguet A., Vacher L., Relexans S., Saubusse S., Froidefond J. M., Parlanti E., 2009. Properties of fluorescent dissolved organic matter in the Gironde Estuary. Organic Geochemistry. 40 (6): 706-719.

Idso S. B. J. L., Oceanography, 1973. On the concept of lake stability1. 18: 681-683.

Lawson R., Anderson M. A., 2007. Stratification and mixing in Lake Elsinore, California: An assessment of axial flow pumps for improving water quality in a shallow eutrophic lake. Water Research. 41 (19): 4457-4467.

Lee M.-H., Osburn C. L., Shin K.-H., Hur J., 2018. New insight into the applicability of spectroscopic indices for dissolved organic matter (DOM) source discrimination in aquatic systems affected by biogeochemical processes. Water Research. 147: 164-176.

McKnight D. M., Boyer E. W., Westerhoff P. K., Doran P. T., Kulbe T., Andersen D. T., 2001. Spectrofluorometric characterization of dissolved organic matter for indication of precursor organic material and aromaticity. Limnology and Oceanography. 46 (1): 38-48.

Ohno T., 2002. Fluorescence Inner-Filtering Correction for Determining the Humification Index of Dissolved Organic Matter. Environmental Science & Technology. 36 (4): 742-746.

Parlanti E., Wörz K., Geoffroy L., Lamotte M., 2000. Dissolved organic matter fluorescence spectroscopy as a tool to estimate biological activity in a coastal zone submitted to anthropogenic inputs. Organic Geochemistry. 31 (12): 1765-1781.

Shi J.-C., Huang T.-L., Wen G., Liu F., Qiu X.-P., Wang B.-S., 2016. The Variation Characteristic of Sulfides and VOSc in a Source Water Reservoir and Its Control Using a Water-Lifting Aerator. International Journal of Environmental Research and Public Health. 13 (4): 427.

Weiying F., Lixin J., Sheng Z., Liming W., Xujin F., Changyou L., Fengli C., 2013. Spectral characteristics of dissolved organic matter in the sediments of Wuliangsuhai Lake. China Environmental Science. 33 (6): 1068-1074 (in Chinese).

Zhou Z., Guo L., Shiller A. M., Lohrenz S. E., Asper V. L., Osburn C. L., 2013. Characterization of oil components from the Deepwater Horizon oil spill in the Gulf of Mexico using fluorescence EEM and PARAFAC techniques. Marine Chemistry. 148: 10-21.

Zsolnay A., Baigar E., Jimenez M., Steinweg B., Saccomandi F., 1999. Differentiating with fluorescence spectroscopy the sources of dissolved organic matter in soils subjected to drying. Chemosphere. 38 (1): 45-50.